2021 43rd Annual International Conference of the
IEEE Engineering in Medicine & Biology Society (EMBC)
Oct 31 - Nov 4, 2021. Virtual Conference

Ultra Low Power Photometry for Pulse Oximetry Applications*

John O'Donnell, John Nelson

***Abstract*— Removing patient cables from the hospital environment, through the use of wireless sensors, improves hygiene, convenience and standard-of-care [1] [2]. In the drive to eliminate cable clutter, vital signs monitoring (VSM) is "going wireless." This, in turn, is driving a trend for battery powered VSM sensors such as Saturation of Peripheral Oxygen (SpO2), Blood Pressure (BP), and Electro-cardiogram (ECG) sensors with a resultant demand for ultra-low-power circuits and algorithms. The architecture of the optical SpO2 pulse oximeter, which measures blood oxygenation and heartrate, is described with a focus on the drivers and contributors to system power. Two concepts for reduction of power in the pulse oximeter are explored. Firstly, an algorithm which modulates LED current according to the instantaneous heartbeat pulse phase is demonstrated in hardware and software. Secondly, an inductor centric LED driver, which provides the power efficiency of a switched mode current source and the system accuracy of a linear current source is introduced with feasibility demonstrated by circuit and system simulation.**

***Clinical Relevance*— The techniques discussed enable longer battery life for the SpO2 wireless VSM which, in turn, improves hygiene, convenience and, most importantly, mobility of the patient in the clinical setting.**

I. Introduction

A pulse oximeter, or SpO2 sensor, measures the oxygen saturation in arterial hemoglobin by employing photometry and exploits two physical phenomena. First, the oxygenated hemoglobin is contained within arteries whose volume has a "pulsatile" component and, second, the relative absorbance of oxygenated and deoxygenated hemoglobin is different in the red and infrared (IR) spectral regions [16].

Fig. 1 shows a typical clinical SpO2 sensor system. Red and infrared (IR) light is passed through the patient (typically the finger or ear) and the transmitted light is detected by a photodiode (PD). Analog and digital signal processing converts the detected light intensities to an oxygen saturation measurement.

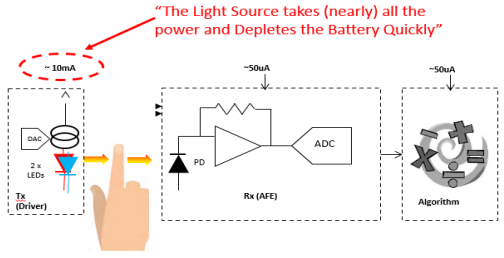

Figure 1. Generic Clinical SpO2 system.

In clinical systems, power is dominated by the LED current, which is of the order of mAs versus uAs for the rest of the system and, as is demonstrated in Fig. 2, has a direct impact on system performance.

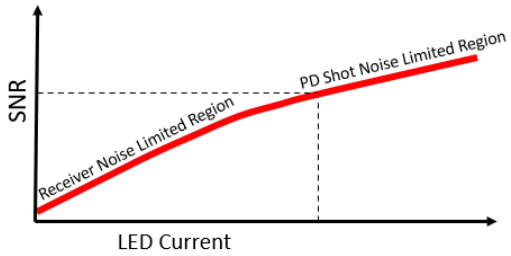

Figure 2. Relationship between SNR and LED current.

Fig. 3 shows the photoplethysmograph (PPG) trace that is received by the system after modulation of the LED light by the finger containing arterial blood. The light received contains unwanted ambient light, the DC component of the LED light which passes through the finger and the small "pulsatile" component which is due to the dilation and contraction of the arteries and capillaries within the finger in response to heartbeat pressure changes.

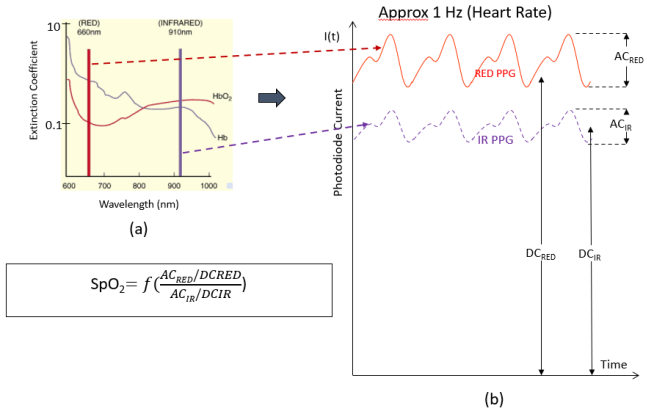

Figure 3. (a) Extinction Coefficients of Hb and HbO2 as a function of wavelength. (b) Typical Red and IR PPG signals.

The SpO_2 measurement is a function of the relative amplitudes of the pulsatile AC components of the red and Infrared PPGs and is given by the following equations [1].

$$SpO2 = \frac{81 - 18R}{0.73 + 0.11R}\% \quad (1)$$

where

*Research supported by Irish Research Council and Analog Devices International.

John O'Donnell is with University of Limerick, Ireland and Analog Devices International. (e-mail: jjodonne2@gmail.com).

John Nelson is with University of Limerick, Ireland. (e-mail: john.nelson@ul.ie).

$$R = \frac{AC_{RED}}{DC_{RED}} \Big/ \frac{AC_{IR}}{DC_{IR}} \quad (2)$$

There are several variations of equation 1 in the literature and system parameter variations mean that a customization of the equation and a one-time calibration is required. The version of the equation used for this study was as follows [3].

$$SpO2 = 117.93 - 10.3 * R^2 - 27.865 * R \quad (3)$$

The algorithm accounts for variations in light intensity, finger thickness, tissue composition, blood perfusion, heartrate, etc. To eliminate ambient light and because the red and IR LEDs must not be illuminated together, the LEDs are typically pulsed [9-12] and alternated in the fashion depicted in Fig. 4.

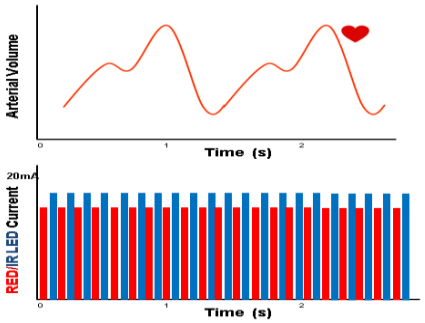

Figure 4. Pulsing of Red and IR LED current.

II. Sources of System Inefficiency

Although, as demonstrated in Fig. 2, the minimum LED current needed for a given system accuracy requirement has a theoretical limit set by the shot noise of the photodiode (PD), system analysis identified sources of power inefficiency and, hence, opportunities to improve system power without compromising performance. They are

1. Photodiode Efficiency (coulombs per photon) is about 60% of theoretical maximum.
2. LED efficiency (photons per coulomb) is only about 18% of theoretical maximum
3. Much of the light emitted by the LED is scattered and is not directed towards the PD.
4. Ambient light adds noise to the system without adding signal, thus reducing signal-to-noise ratio (SNR).
5. The LED control algorithm illuminates the patient tissue equally intensely at all phases of the heartbeat even when light is not required for the SpO2 calculation.
6. The linear LED drivers are, depending on the ratio of supply voltage to LED forward voltage, less than 50% efficient.

The remainder of this paper focuses on methods to mitigate inefficiencies 5. And 6. above.

III. LED Modulation

A. Bench Prototype Setup

A benchtop prototype system was developed for the purpose of algorithm development. The main components of this system, which is shown in Fig. 5, include a PCB containing a microprocessor and an optical analog front end (AFE) device for LED pulsing and PD readout. Low level algorithms for illumination and sensing are implemented on the embedded micro while the higher level SpO2 calculation algorithms are implemented as a post-processing step on a PC.

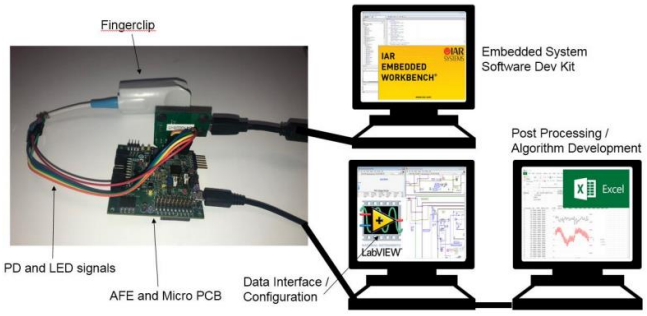

Figure 5. Benchtop Prototype for Algorithm Development

B. Prototype System Operation

In advance of developing a power-saving current modulation algorithm, it was necessary to establish a performance baseline. Using an LED pulsing regime as shown in Fig. 4, and using a human patient, SpO2 was calculated once per heartbeat using processing of the pulsatile maxima and minima of the red and IR PPG traces. The output of this system is shown in Fig. 6. where the classic IR and red PPG traces can be seen along with the calculated SpO2 saturation (updated once per hearbeat). Accuracy over a 100s period is +/- 0.6%.

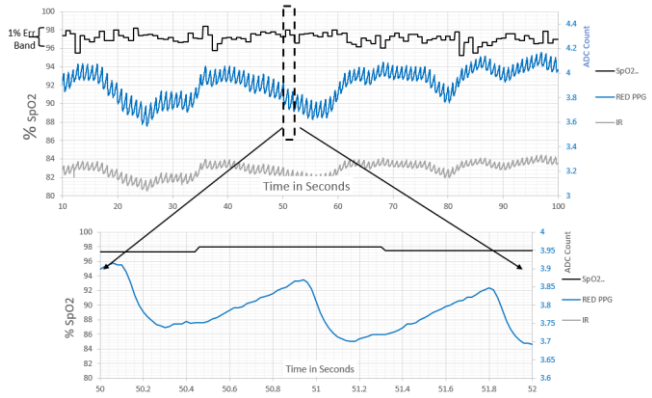

Figure 6. Calculated SpO2, Red PPG and IR PPG traces over a 100s and over a 2 second period.

C. Prototype System Operation

Fig. 7 shows the top-level block diagram of the algorithm implementation for the complete system. The development of the LED modulation algorithm which is highlighted is now described.

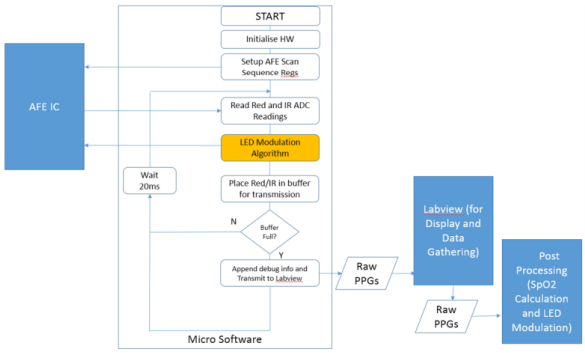

Figure 7. Algorithm implementation block diagram with new LED Modulation algorithm shown

The basis for the algorithm is the observation that only the PPG data at the maxima and minima of the respective IR and red traces are required for the SpO2 calculation. In theory, the LED power consumed at other phases of the heartbeat period are wasted and this point has been exploited in the past by turning off the LEDs for certain portions of the pulsatile period [2]. One drawback of this approach is that, while the LEDs are off, PPG data are no longer being acquired with the resultant loss of phase awareness by the modulation algorithms.

The approach presented here is to *reduce* the intensity of, rather than *turn off*, the LEDs at those times when the algorithm does not require full system accuracy. By reducing the LED intensity to 10% of that required at the PPG maxima and minima and by digitally reconstructing the PPG, the resultant PPG can be used to both retain phase awareness and to accurately calculate the oxygen saturation of the patient. A further benefit is a visual reconstruction of the PPG for the physician.

The concept is demonstrated in Fig. 8, where the red trace shows the LED power setting while the blue trace shows the resultant PPG trace. The missing portions of the PPG are digitally recovered by multiplying the PPG signal by the attenuation factor applied to the LED current in the regions of low intensity.

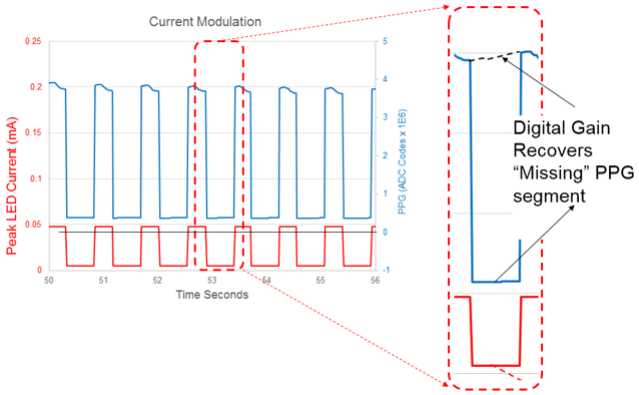

Figure 8. PPG trace (in blue) as a result of modulated pulse energy envelope (red)

The resultant PPG is shown in Fig. 9 and it can be noted that the PPG has noisy and "smooth" portions corresponding to the regions of low LED intensity and high LED intensity respectively. Also shown in this figure is the derivative of the PPG signal from which a large negative deviation indicates the location of the systolic region of the PPG and which proved to be a very reliable reference phase marker for the implementation of the digital PLL which provides continuous tracking of the PPG phase, even during the noisy portions.

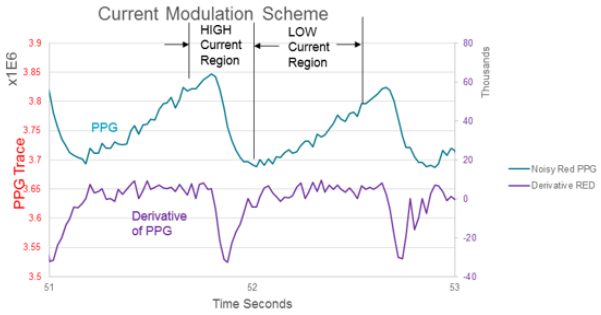

Figure 9. Digitally reconstructed PPG trace, in blue and its first derivative

The main elements of the algorithm are shown in Fig. 10. After restoration of the PPG where the effects of the LED current modulation are removed, feature detection and phase locking provide heartbeat phase awareness which is then used by the LED pulser to determine whether the next pulse should be low power or high power.

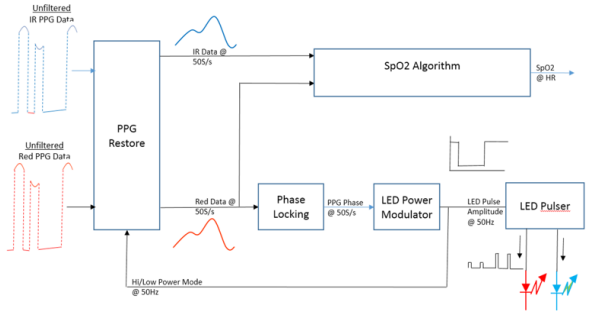

Figure 10. Main elements of LED modulation algorithm.

D. *Performance of system with LED current modulation*

Fig. 11 shows the analogue of Fig. 6 with current modulation running. The system is performing with an accuracy of +/-0.5%, as before.

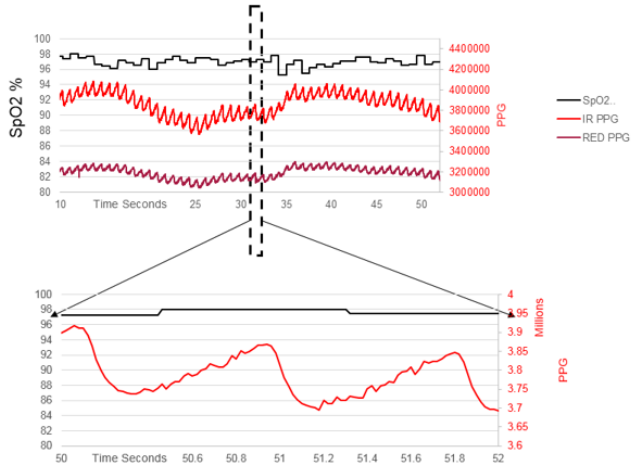

Figure 11. Calculated SpO2 (per heartbeat) and red reconstructed PPG.

The average power consumed by the red and IR LEDs and LED drivers was 2.8 mW when in high power mode and 0.44mW when in low power mode. With a high power to low power duty cycle of 44%, this equated to a 47% reduction in LED driver power without loss of performance.

IV. Switched Mode LED Driver Concept

Fig. 12 shows two ways in which power is wasted in the LED driver circuits. Firstly, IR drop across the current source results in dissipation within the driver itself. Even if the supply voltage is optimized using an external DCDC converter, the headroom required by the LED driver in order to provide a sufficiently noise-free current is of the order of 1V. Secondly, several microseconds of LED pulse settling are required before PD readings can commence. This is due to the ringing caused by inductive parasitics.

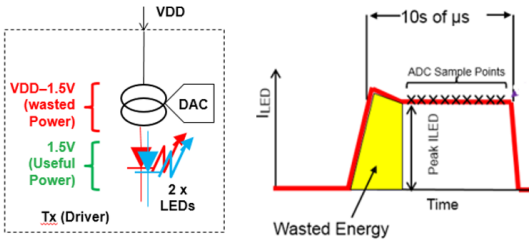

Figure 12 – Wasted power in pulsed LED system caused by (a) IR drop and (b) pulse settling

While nearly all of the systems in the literature have used linear LED drivers, there have been attempts [6-8] to employ inductors. These have been proposed for heartrate monitors but problems remain in integrating them into SpO2 systems. Although switched mode LED drivers are common in the LED lighting domain, they are not employed in spectro-photometry systems for the following reasons.

1. Current is too noisy to use in a >90dB measurement system.
2. The power supply rejection ratio (PSRR) is extremely bad, and the same battery typically drives other noisy loads in the system (such as the radio.)

The system outlined in Fig. 13 solves both these issues while improving the power efficiency to that of a switched mode driver.

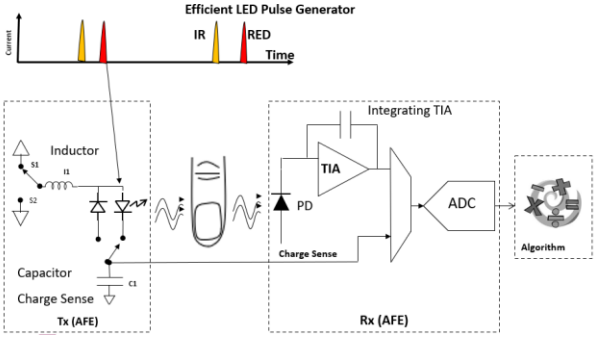

Figure 13. System utilizing a switched mode LED driver.

The system shown has the following features and benefits.

1. An inductor for power efficiency.
2. An integrating transimpedance amplifier (TIA) which ensures that every photon detected by the PD is counted and, more importantly, renders the system immune to variations in the pulse shape. The system, unlike the one shown in Fig. 1 which is a current centric receiver, is a charge centric receiver.
3. A capacitor, C1, which collects every coulomb of charge that flows through the LED during each pulse event. Measurement of the step voltage on this capacitor is a direct measurement of the pulse energy and is used by the algorithm to compensate for any fluctuations in the pulse energy due to noise or power supply interference.

A. Operation of the circuit

Assuming that the initial capacitor voltage is 0V, closing of the switch S1 causes a current pulse with a sinusoidal half cycle shape to flow through the red LED. The critical parameters of this pulse are given by the following equations.

$$Pulse\ Width = \frac{\pi}{\omega} = \pi\sqrt{LC}\ s \quad (4)$$

$$Charge\ Q = (V_{DD} - V_F) * \sqrt{\frac{C}{L}} \int_0^{\frac{\pi}{\omega}} \sin \omega t dt \ \text{Coulombs} \quad (5)$$

$$Charge\ Q = (V_{DD} - V_F) * 2C \ \text{Coulombs} \quad (6)$$

$$LED\ Energy = (V_{DD} - V_F) * 2C * V_F \ \text{Joules} \quad (7)$$

$$C1\ Stored\ Energy = (V_{DD} - V_F) * 2C * V_C \ \text{Joules} \quad (8)$$

where L is the inductor value, C is the capacitor value and ω is the natural frequency of the LC tank.

A similar pulse is generated through the IR LED, flowing from the capacitor when S2 is closed along with the switch connecting the IR LED to the capacitor.
It is interesting to note that pulse energy is determined only by the capacitor value and voltage headroom while pulse width, and hence peak current, is a function of both capacitor and inductor values. The selection of the capacitor and inductor values put an upper limit on pulse width and energy, and the regulation of these parameters is achieved by a switch timing circuit and a power regulation and control algorithm not described in this paper. The controller also enables fast switching between high energy and low energy pulses as required by the algorithm in the first section of this paper.

B. Simulation Results

Fig. 14 shows the PPG waveforms from the full system simulation. Corruption of the PPG by supply noise has been removed by the digital compensation algorithm which uses the pulse energy monitor data from the C1 capacitor voltage monitor.

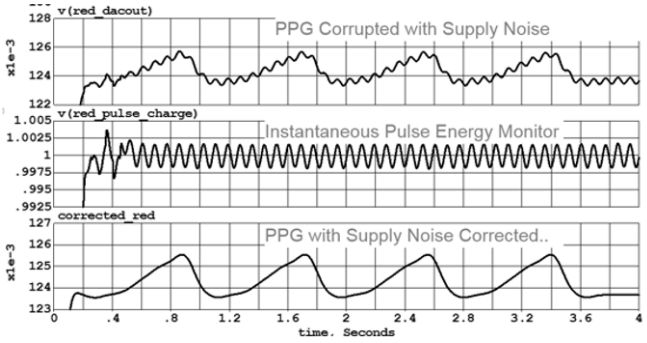

Figure 14. Simulation waveforms - corrupted and digitally corrected PPG.

Table 1 shows the results of the simulations of the linear and switched-mode systems with an improvement of nearly 3x in system efficiency (under the operating conditions chosen) and a complete removal of the negative performance impacts through the use of pulse energy monitoring and compensation.

TABLE I. SUMMARY OF SWITCHED MODE SYSTEM PERFORMANCE

	SpO2 Accuracy (% SpO2)	Efficiency
Linear System (State of the Art)	0.2	36% (27% including pulse settling)
Switched Mode System		
- With 20mV (pkpk) Supply Noise	4	91.5% *
- With 140mV (pkpk) Supply Noise	30	91.5%
Switched Mode System with PPG Correction and enhanced peak detection		
- With 20mV (pkpk) Supply Noise	0.06	91.5% **
- With 140mV (pkpk) Supply Noise	0.1	91.5%

* Efficiency improved but SpO2 accuracy compromised
** Efficiency improved and SpO2 accuracy recovered

V. CONCLUSION

Two new concepts for power optimization in a battery powered clinical pulse oximeter system are presented with each achieving an approximately 50% reduction in system power. This gives a combined system power reduction of 75% without compromising system performance.

ACKNOWLEDGMENT

The authors would like to acknowledge the assistance and guidance of Javier Calpe, Colin Lyden, Mike Coln, Tom O'Dwyer, and Donal Geraghty of Analog Devices.

REFERENCES

[1] D. Freeman, "The Future of Patient Monitoring," *Health Management Technology,* vol. 30, p. 1, 2009.

[2] A. Pedersen, "GE aims to make wireless patient monitoring systems," *Medical Device Daily,* vol. 13, p. 2, 2009.

[3] K. N. Glaros and E. M. Drakakis, "A Sub-mW Fully-Integrated Pulse Oximeter Front-End," *Biomedical Circuits and Systems, IEEE Transactions on,* vol. PP, pp. 1-1, 2012.

[4] S. V. Gubbi and B. Amrutur, "Adaptive Pulse Width Control and Sampling for Low Power Pulse Oximetry," *Biomedical Circuits and Systems, IEEE Transactions on,* vol. 9, pp. 272-283, 2015.

[5] T. Bheema et al, "Measurement of Pulse rate and SPo2 using Pulse Oximeter developed using LabVIEW," IOSR Journal of Electrical and Electronics Engineering, Volume 8, Issue 1, 2013.

[6] W. Saadeh, T. Tekeste, and M. H. Perrott, "A > 89% efficient LED driver with 0.5V supply voltage for applications requiring low average current," in *Solid-State Circuits Conference (A-SSCC), 2013 IEEE Asian*, 2013, pp. 273-276.

[7] W. Saadeh, S. Z. Aslam, A. Hina, and F. Asghar, "A 0.5V PPG-based Heart Rate and Variability Detection System," in *2018 IEEE Biomedical Circuits and Systems Conference (BioCAS)*, 2018, pp. 1-4.

[8] B. Chew, "Switch-Mode Oximeter LED Drive With a Single Inductor," US Patent 8195262, June 5th, 2012.

[9] E. S. Winokur, T. O'Dwyer, and C. G. Sodini, "A Low-Power, Dual-Wavelength Photoplethysmogram (PPG) SoC With Static and Time-Varying Interferer Removal," *IEEE Transactions on Biomedical Circuits and Systems,* vol. 9, pp. 581-589, 2015.

[10] H. Zhang and Y. Li, "A Low-Power Dynamic-Range Relaxed Analog Front End for Wearable Heart Rate and Blood Oximetry Sensor," *IEEE Sensors Journal,* pp. 1-1, 2018.

[11] H. Chen, S. Hsieh, T. Hsu, and C. Hsieh, "A CMOS Imager for Reflective Pulse Oximeter with Motion Artifact and Ambient Interference Rejections," in *2018 IEEE Asian Solid-State Circuits Conference (A-SSCC)*, 2018, pp. 25-26.

[12] Y. Lee, H. Lee, J. Jang, J. Lee, M. Kim, J. Lee, *et al.*, "22.3 A 141μW sensor SoC on OLED/OPD substrate for SpO2/ExG monitoring sticker," in *2016 IEEE International Solid-State Circuits Conference (ISSCC)*, 2016, pp. 384-385.

[13] D. Dempsey, S. Brennan, J. O'Donnell, and C. Lyden, "Transconductance circuit and a current digital to analog converter using such transconductance circuits " USA Patent 9203350, Dec 1st, 2015.

[14] J. O'Donnell, J. Calpe, C. Lyden, T. O'Dwyer, "Blood Oxygenation Sensor with LED Current Modulation," USA Patent 10582887, 2020.

[15] J. O'Donnell, C. Lyden, M. Coln "Systems and Methods for Measuring Oxygen in a Patient's Bloodstream", USA Patent Application, US20200245915, 2020.

[16] P. Tilakaratna. "*How Medical Equipment Works - Pulse Oximetry*" Available: https://www.howequipmentworks.com/pulse_oximeter/ 2016.